INVESTIGATIONS OF NANOPARTICLES FOR OPTICAL POWER LIMITING

Stefanie Dengler[(1)], Olivier Muller[(2)], Günter Straube[(3)], Gunnar Ritt[(1)], Bernd Eberle[(1)]

[(1)]) Fraunhofer Institute of Optronics, System Technologies and Image Exploitation IOSB, Departement Optronics, Gutleuthausstrasse 1, 76275 Ettlingen, Germany, Email: stefanie.dengler@iosb.fraunhofer.de

[(2)] French-German Research Institute of Saint-Louis, Optronics & Laser Applications – Division 3, 5 rue du Général Cassagnou – BP 70034, 68301 Saint-Louis Cedex, France, Email: olivier.muller@isl.eu

[(3)] Wehrwissenschaftliches Institut für Schutztechnologien - ABC-Schutz, Humboldtstrasse 100, 29633 Munster, Germany, Email: guenterstraube@bwb.org

ABSTRACT

In order to study the properties of potential materials for optical limiting, i.e. the nonlinear transmittance of the various suspensions, we conducted experiments with short (ns) and ultra-short (ps) laser pulses in the visible and near infrared spectral region. Three different laser systems were used: A Coherent Infinity Nd:YAG laser system with a pulse duration of 3 ns, a SPECTRON SL400 Nd:YAG laser system with 7 ns, both working at a wavelength of 1064 nm or 532 nm, and a HighQ picoRegen IC-2500 Nd-YLF laser system with a pulse duration of 8 ps, working at a wavelength of 1053 nm or 526.5 nm.

As optical power limiting materials, we investigated different kinds of carbon-based nanomaterials and metallic nanostructures suspended in a solvent. Among them, we studied the nonlinear properties of gold nanoparticles, multi walled carbon nanotubes (MWCNT), carbon black (CBS) and C_{60}, the best known representative of the fullerene family.

The nanoparticles were characterized regarding their geometry dependent linear optical properties by spectral transmission measurements and geometrical structure by electron microscopy. The nonlinear behavior of the suspensions at the interaction with short and ultra-short laser pulses is discussed.

1. INTRODUCTION

The protection of eyes and electro-optical sensors against wavelength agile pulsed laser radiation is still a demanding problem, which has not been solved sufficiently during the past decades. Contrary to that, laser protection against known wavelengths is a trivial problem. One can use classical absorption or interference filters.

Since laser pulses may have rise times of nanoseconds or even below, one needs passive, self-acting devices which limit the transmitted power of light. Such devices are known as optical power limiters [1],[2]. They can be based on nonlinear optical materials and shall fulfill a number of essential requirements over a broad spectral range. In detail that is: fast response time, low nonlinear threshold, color neutrality, efficient limitation in the wavelength range of interest and high linear transmittance.

Recently, nanomaterials have attracted much interest due to their strong and often broadband nonlinear optical behavior [3]-[5]. Especially gold, silver and carbon based nanoparticles have been widely studied and are the nowadays benchmark materials for optical limiting nanomaterials. The rapid progresses in physical and chemical production methods have opened the opportunity to design specific nanoparticles with a narrow size-distribution and with defined surface properties.

2. EXPERIMENTAL

2.1. Sample Preparation

The nanopowders MWCNT (Pyrograph III, Sigma Aldrich), C_{60} (99.99%, Sigma Aldrich) and CBS (synthesized at ISL laboraties) were suspended in different solvents: MWCNT in chloroform, C_{60} in toluene and CBS in ethanol.

The gold (Au) cubes were prepared using a synthesis method reported by Hiramatsu and Osterloh [6] with minor changes. Briefly, chlorauric acid ($HAuCl_4$, Sigma Aldrich) (0.25 mmol) was dissolved in 370 µl oleylamine (Sigma Aldrich)

and 100 µl toluene (Merck). The nanoparticles were obtained by quickly adding the $HAuCl_4$ solution into a boiling mixture of 630 µl oleylamine and 5 ml toluene. The resultant mixture was refluxed 2 h under stirring at 120°C. 10 ml methanol (Merck) was added to precipitate the particles followed by centrifugation. After three washing cycles with distilled water and ethanol (Merck) the particles were redispersed in methyl 2-methylprop-2-enoate.

The branched Au nanoparticles were synthesized by a sodium diphenylamin-4-sulfonate reduction process [7]. In brief, 1 ml polyethylene glycol (PEG, Mw 400, Alfa Aesar) was added into 30 ml of an aqueous sodium diphenylamin-4-sulfonate (SDS, Sigma Aldrich) solution (0.8 mM). After 30 minutes 2.5 ml aq. $HAuCl_4$ solution (0.035 M) was added and stirred for 24 h at room temperature. The particles were also collected by centrifugation, washed three times and redispersed in methyl 2-methylprop-2-enoate.

All samples were diluted to have a linear transmittance between 50% and 60% at 532 nm.

2.2. Experimental Details

The experimental setup used to study the optical limiting properties of the samples (nonlinear attenuation or transmittance) is shown schematically in Figure 1. We used a Q-switched Nd:YAG laser (Coherent Infinity) working at a wavelength of 1064 nm or 532 nm, with a pulse width of 3 ns, a Q-switched Nd:YAG laser (SPECTRON SL400) with 7 ns, both at a repetition rate of 3 Hz and a HighQ picoRegen IC-2500 Nd-YLF laser system with a pulse duration of 8 ps, working at a wavelength of 1053 nm or 526.5 nm. The pulse repetition was set to 10 Hz in all ps experiments. To simulate far-field conditions the original 5 mm flattop laser beam was expanded with a 6.7x Galilean telescope before entering the Keplerian telescope. The entrance aperture A1 was overfilled by the expanded laser beam resulting in a beam with a top-hat spatial irradiance distribution. The samples were placed in the intermediate image plane of the Keplerian telescope formed by the lenses L1 and L2 (focal length 60 mm and 100 mm). In front of the input lens L1 and behind the output lens L2 the apertures A1 and A2 (diameter 12 mm and 20 mm) were placed to provide an optical system with f-number f/5. The focal diameters in the 3 ns setup were determined in air by the knife-edge method to be 4 µm at 532 nm and 8 µm at 1064 nm. At 532 nm the focal diameter was determined in addition by a beam profiler (DataRay WinCamD-UCM) with the help of a microscope objective (Mitutoyo M Plan Apo NIR 50x) and an achromatic doublet lens (focal length 150 mm) and gave the same result. The diameters at the 7 ns setup were measured to be 7 µm at 532 nm and 10 µm at 1064 nm.

In order to monitor the incident pulse energy, a part of the laser beam was split off by means of a beam splitter BS. To identify the residual hazardous energy transmitted through the sample, the focusable energy (or encircled energy) was measured. The focusable energy is defined in general as the energy detected within a solid angle of 1.5 mrad [8]. This was achieved using the lens L3 (focal length 400 mm) and the pinhole A3 (diameter 600 µm) in front of the signal photo diode.

The experimental set-up for the ps measurements was equivalent to that one of the ns experiments. The focal spot size of the laser beam was approximately 5 µm at the wavelength of 526.5 nm and approximately 10 µm at the wavelength of 1053 nm.

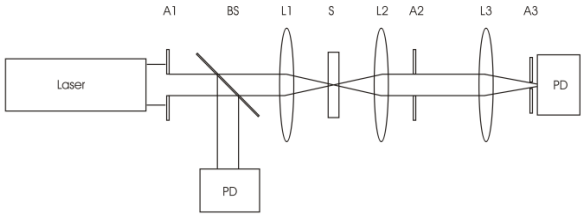

Figure 1: Experimental setup to study the nonlinear transmittance. L1, L2, L3 - lenses; S - sample; PD - photodiode; BS - beamsplitter; A1, A2, A3 – apertures.

In order to characterize the spectral optical properties of the nanoparticle samples we used a Shimadzu UV-3600 UV-VIS-NIR spectrophotometer. A quartz cuvette with a 10 mm optical path length was used to measure the transmittance in the VIS-NIR spectral range and to measure the nonlinear transmittance in the laser setup.

Since the optical properties of the nanoparticles are related to their geometrical and morphological characteristics, the samples were further analyzed by transmission and scanning electron microscopy (TEM and SEM). SEM images of the metallic nanoparticles were taken using a Zeiss Supra 40 VP with an InLens detector at a working distance

of 2 mm, operated at 1.5 kV, TEM images using a Zeiss EM 902 at an accelerating voltage of 80 kV. The micrographs of the different carbon particles were taken with a ZEISS DSM 982 at a working distance of 5 mm operated at 10 kV.

The samples were prepared by placing a droplet of the suspended metal nanoparticles onto a substrate and dried in air. We used a carbon copper grid (Plano) for TEM measurements and a silicon wafer (Plano) for SEM characterization. The SEM samples were sputter coated in addition with palladium-platinum.

3. RESULTS AND DISCUSSION

3.1 Optical Characterization

The transmittance of MWCNT and CBS samples between 400 nm and 1100 nm is quasi constant, whereas C_{60} has an increased absorption around 550 nm, due to ground state excitation (Figure 2).

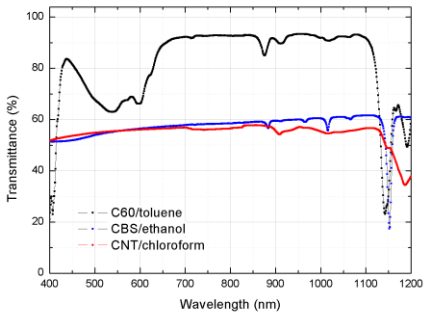

Figure 2: VIS-NIR spectra of C_{60}, CBS and CNT.

The spectra of the various Au samples are shown in Figure 3. In order to study the growth process of Au branched particles, spectra were recorded at different times during the synthesis (1 h, 6 h, 18 h, 24 h). These spectra show two surface plasmon resonance (SPR) peaks around 500 nm and 950 nm. The spectrum after 1 h has a less pronounced longitudinal band (around 950 nm) which increases during the reaction time.

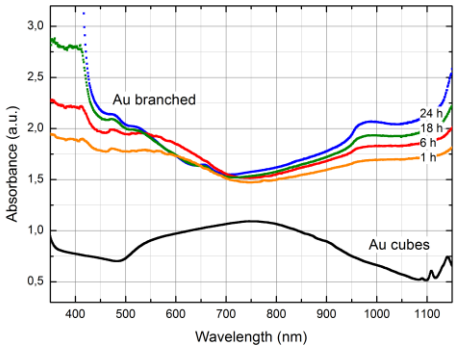

Figure 3: VIS-NIR spectra of branched and cubic shaped Au particles. In the case of the branched nanocrystals the spectral change during the synthesis was studied.

3.2 Electron Microscopy

Figure 4 shows the SEM image of MWCNT. Their size is a few micrometers in length and 100 nm in diameter. Typical grape-like coagulations of CBS particles can be seen in Figure 5.

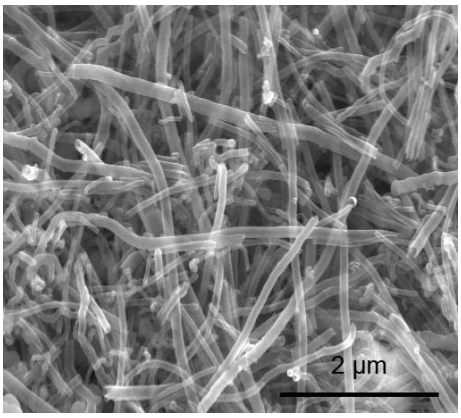

Figure 4: SEM image of MWCNT at 20000 X magnification.

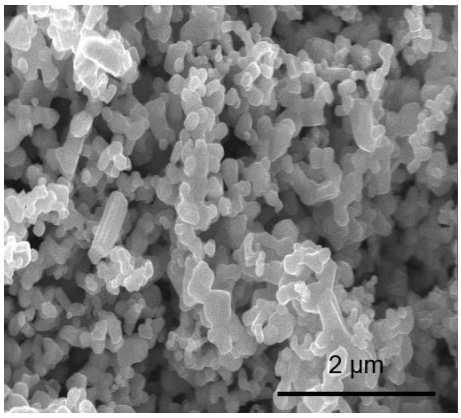

Figure 5: SEM image of grape-like coagulations of CBS at 20000 X magnification.

Figure 6 shows the SEM images of Au cubes at 10.00 kX magnification (top) and 50.00 kX magnification (bottom) magnification. The cubic shaped particles with an edge length of around 80 nm exhibit a very narrow size distribution.

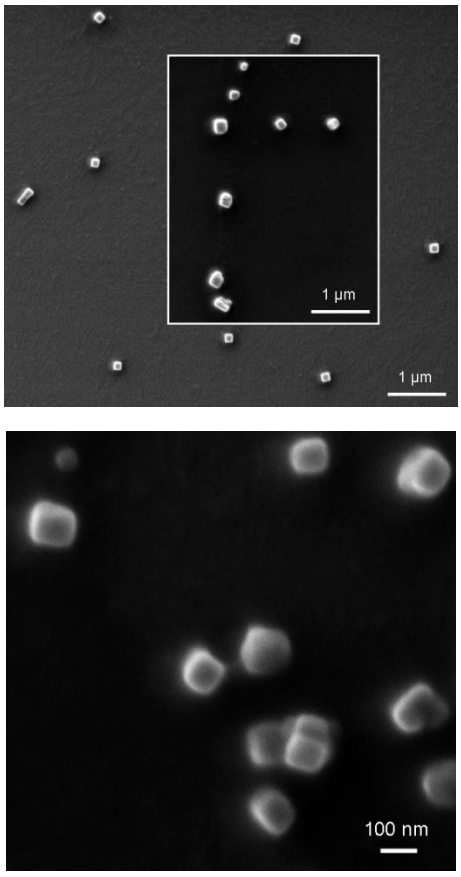

Figure 6: SEM images of Au cubes at different magnifications.

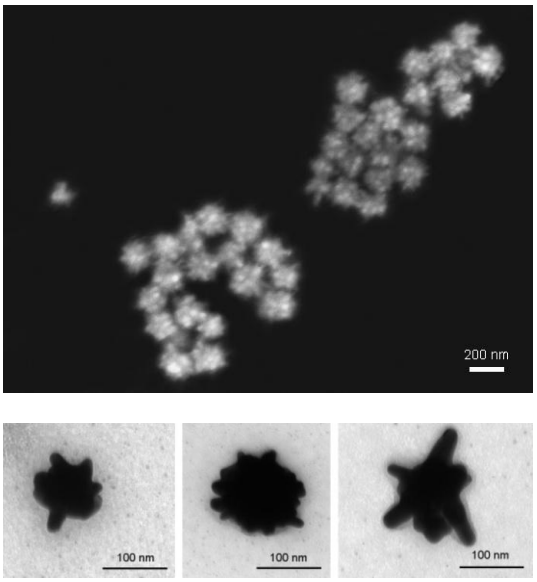

Figure 7: SEM (top) and TEM (bottom) images of Au branched particles.

In Figure 7 multibranched Au particles are shown: SEM image (top) at 20.00 kX magnification and TEM images (bottom). The branched particles have a size comparable to the cubes. As in the case of the cubes their size distribution is also very narrow.

3.3 Optical Limiting Properties

3.3.1. Carbon Based Structures

The normalized transmittance results of MWCNT are given in Figure 8. For ps laser pulses the limiting curves of chloroform and MWCNT in chloroform are nearly congruent. Thus we can conclude that there is no limiting effect by MWCNT in the ps time domain. On the other hand at ns pulses the nonlinear threshold, defined as the 50% drop in transmittance, and the attained attenuation of MWCNT is quite better compared to the solvent. (ns: 39.5 J/cm^2 at 532 nm and at 1064 nm, ps: 7.6 J/cm^2 at 526.5 nm). These results could be expected since the main limiting mechanism of MWCNT is nonlinear scattering [9]. The particles act as scattering centers due to sublimation. In addition there occurs a heat transfer to the surrounding, which leads to a solvent bubble-growth. These bubbles are called second type scattering centers. With a growth rate of about 200 nm/ns it takes approximately 1 ns to establish significant scattering centers [10]. Therefore, in the ps pulse regime nonlinear scattering does not contribute to optical power limiting and only the reaction of the solvent is observed.

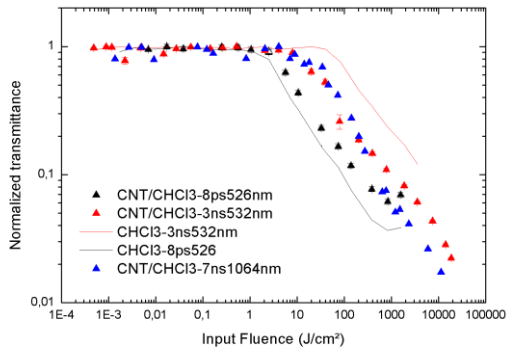

Figure 8: Normalized transmittance as a function of the input fluence (log-log scale) of MWCNT in chloroform for ns laser pulses at 532 nm and 1064 nm and for ps laser pulses at 526.5 nm. The solid lines show the behavior of the pure solvent.

CBS show the same behavior as the MWCNT samples (Figure 9). At ps pulses the attenuation is equivalent to the solvent, whereas at ns pulses the optical limiting properties are enhanced compared to the solvent. The main limiting mechanism at ns pulses is also nonlinear scattering [11]. The nonlinear thresholds of CBS particles at 7 ns are: 150 J/cm² for 1064 nm, and at 8 ps: 80 J/cm² for 526.5 nm and 1053 nm:

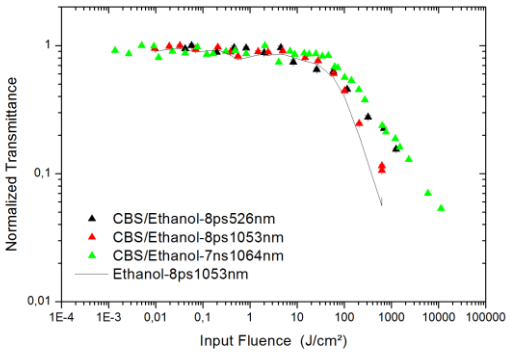

Figure 9: Normalized transmittance as a function of the input fluence (log-log scale) of CBS in ethanol for ns laser pulses at 1064 nm and for ps laser pulses at 526.5 nm and 1053 nm. The solid line shows the behavior of the pure solvent.

CBS as well as MWCNT show no additional influence on the nonlinear transmittance characteristic at ps pulses compared to the pure solvent. Thus the shape of the nonlinear curve results from the solvent alone.

In summary, the nonlinear threshold and attenuation of MWCNT are better compared to CBS. This is explained by the fact that the nonlinear scattering efficiency depends on the specific surface of the particles [12].

C_{60} suspensions exhibit an optical limiting effect in the visible range at ns and ps pulse durations. Conversely the NIR laser radiation is ineffectively limited.

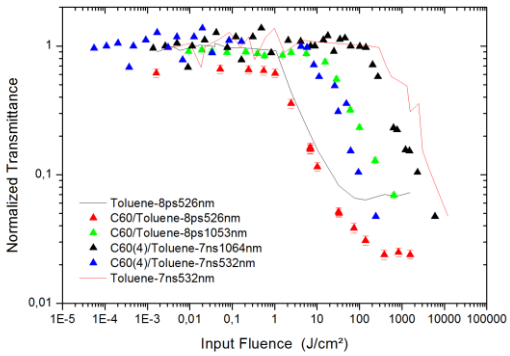

Figure 10: Normalized transmittance as a function of the input fluence (log-log scale) of C_{60} in toluene for ns laser pulses at 532 nm and 1064 nm and for ps laser pulses at 526.5 nm and 1053 nm. The solid lines show the behavior of the pure solvents.

In the case of C_{60} the main limiting mechanism is reverse saturable absorption (RSA) [13]. Our experimental data are in agreement with a five-level RSA-model, which describes the narrowband limitation nature of C_{60}. Electrons can only be promoted to excited states at wavelengths between 400 nm and 700 nm. From there they can be excited to a higher singlet state or relax by intersystem crossing to the lowest triplet state, with subsequent excitation to higher triplet states.

The transmittance properties at ns pulses can mainly be attributed to triplet state absorption, while at ps pulses only excited singlet state absorption occurs.

The nonlinear thresholds of C_{60} at 7 ns are: 300 J/cm² for 1064 nm and 15 J/cm² for 532 nm. At 8 ps they are: 1.5 J/cm² for 526.5 nm and 30 J/cm² for 1053 nm.

The optical limiting properties (nonlinear threshold and attenuation) of C_{60} in the visible range are better than those measured for MWCNT. Due to the inherent electronic structure of C_{60} its limiting properties in the near infrared region is worse. Table 1 gives an overview on the limiting thresholds of the investigated carbon particles.

	Nonlinear threshold (J/cm²)			
	ns pulses		ps pulses	
Sample	532 nm	1064 nm	526.5 nm	1053 nm
CBS		150	80	80
MWCNT	39.5	39.5	7.6	
C_{60}	15	300	1.5	30

Table 1: Summary of the nonlinear thresholds of CBS, MWCNT and C_{60} nanoparticles

3.3.2. Metallic Nanostructures

The nonlinear transmittance curves of the metallic structures (Au cubes and Au branched) at ns pulses are shown in Figure 11. The nonlinear properties of the suspensions at the wavelengths of 532 nm and 1064 nm are by far better than those obtained for the pure solvent.

The nonlinear thresholds for ns-pulses are: 175 J/cm^2 for Au cubes and Au branched particles at 532 nm and 66 J/cm² for Au branched and 115 J/cm² for Au measured cubes both at 1064 nm. The transmittance of Au branched particles decreases more rapidly, which leads to a higher attenuation.

The optical limiting mechanism can be mainly attributed to inter- and intraband transitions, followed by an excited states absorption, which is similar to reverse saturable absorption in molecular systems [14]-[17]. The properties of these particles are determined by d and s-p conduction band electrons. The Au cubes show a small increase of about 5 % in transmittance at low input fluence, also referred to as plasmon band bleach, which is typical for metal nanoparticles.

The performance of gold nanoparticles depends strongly on the particle size [18]-[20]. The gold cubes and gold branched nanostructures used in our work had about the same size. Therefore, the better properties of branched Au could be assigned to the geometry of the particles.

Table 2 gives an overview on the limiting thresholds of the investigated Au particles.

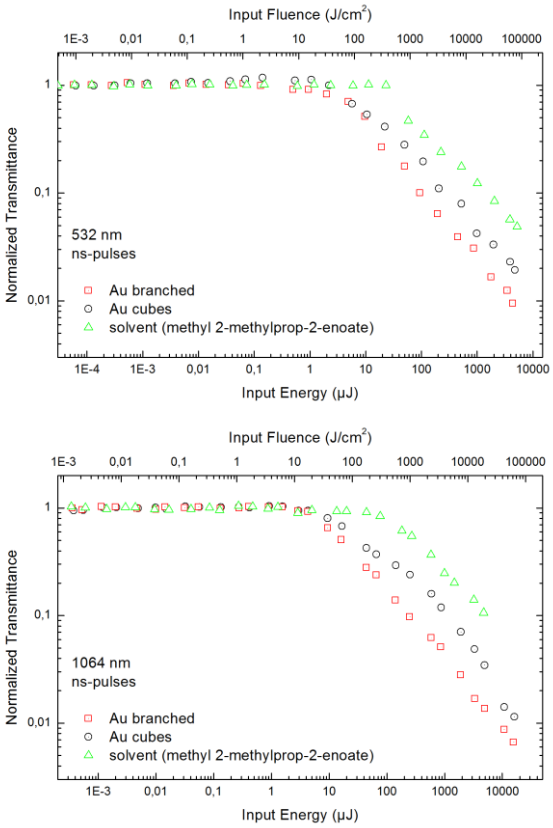

Figure 11: Normalized transmittance as a function of the input laser energy and input fluence (log-log scale) of branched and cubic gold nanoparticles in methyl 2-methylprop-2-enoate at 532 nm (top) and 1064 nm (bottom) ns pulses.

	Nonlinear threshold (J/cm²)	
	ns pulses	
Sample	532 nm	1064 nm
Au cubes	115	175
Au branched	66	175

Table 2: Nonlinear thresholds of Au branched and Au cubic particles.

4. CONLUSIONS

The optical limiting properties of different geometrically shaped nanoparticles, based on the elements carbon or gold, were studied in the nanosecond and picosecond time regimes.

It has been revealed that MWCNT and CBS act as broadband limiters but only in the nanosecond time domain. Due to the higher specific surface MWCNT performs better than CBS. In the case of C_{60} a different optical behavior was observed. Due to its electronic properties optical limiting takes place only in the visible range, but in contrast to MWCNT or CBS it works very well in the time regimes of nanosecond and also picosecond laser pulses.

Our investigations on novel gold structures like cubed or branched particles showed that the limitation efficiency depends on the particle morphology. We observed a broadband limiting effect for both metallic nanostructures. Moreover the branched gold particles had a higher attenuation compared to the cubes. This might be owed to the fact that the interaction of the electric field with the particles depends on their geometrical structure.

5. REFERENCES

[1] Tutt, L. W., Boggess & T. F., (1993). Progr. Quant. Electr. **17**, 229-338

[2] Sun, Y.-P. & Riggs, J. E., (1999). J. Phys. Chem. **18**, 43-90

[3] J. Wang & W. J. Blau, J. Opt. A 11, (2009) 024001

[4] Dengler, S., Ritt, G. & Eberle B., (2009). Proc. of SPIE Vol. 7481 74810T-1

[5] Ganeev, R. A. & Ryasnyansky, A. I., (2006). Appl. Phys. B **84**, 295-302

[6] Hiramatsu, H. & Osterloh, F. E. (2004). Chem. Mater. **16** (13), 2509-2511

[7] Qi, L., Lifang, L., Hexiang, H., Jianhua, S., Tongming, H., Ouanfa, Z. & Zheng, X. (2010). Chin. J. Chem. **28**, 537-542

[8] Hollins, R. C, (1999). Curr. Opin. Solid St. M. **4**, 189-196

[9] Vivien, L., Riehl, D., Delouis, J. F., Delaire, J. A., Hache, F. & Anglaret, E., (2002). J. Opt. Soc. Am. B **19**, 2, 208-214

[10] Vincent, D., Petit, S. & Chin, S. L., (2002). Appl. Opt. **41**, 15, 2944-2946

[11] Hernandez, F. E., Shensky III, W., Cohanoschi, I., Hagan, D. J. & van Stryland, E. W. (2002). Appl. Opt. **41**, 6, 1103-1107

[12] Vivien, L., Lancon, P., Riehl, D., Hache, F. & Anglaret, E., (2002). Carbon **40**, 1789-1797

[13] McLean, D. G., Sutherland, R. L., Brant, M. C., Brandelik, D. M., Fleitz, P. A. & Pottenger, T., (1993). Opt. Lett. 18, 11, 858-860

[14] Jiang, X. C., Brioude, A. & Pileni, M. P., (2006). Colloids and Surfaces A: Physicochem. Eng. Aspects **277**, 201–206

[15] Anija, M., Thomas, J., Singh, N., Sreekumaran Nair, A., Tom, R. T., Pradeep, T. & Philip, R. (2003). Chem. Phys. Lett. **380**, 223-229

[16] Seo, J. T., Yang, Q., Kim, W.-J., Heo, J., Ma, S.-M., Austin, J., Yun, W. S., Jung, S. S., Han, S. W., Tabibi, B. & Temple, D., (2009). Opt. Lett. **34**, 3, 307-309

[17] Martin, R. B., Meziani, M. J., Pathak, P., Riggs, J. E., Cook, D. E., Perera, S. & Sun, Y.-P., (2007). Opt. Mater. **29**, 788–793

[18] Gao, Y., Chang, Q., Ye, H., Jiao, W., Li, Y., Wang, Y., Song, Y. & Zhu, D. (2007). Chem. Phys. **336**, 99-102

[19] Francois L., Mostafavi, M., Belloni, J. & Delaire, J.A., (2001). Phys. Chem. Chem. Phys. **3**, 4965-4971

[20] Francois, L., Mostafavi, M., Belloni, J., Delouis, J.-F., Delaire, J. & Feneyrou, P. (2000). J. Phys. Chem. B **104**, 6133-6137